Macromolecules

Article

pubs.acs.org/Macromolecules

Understanding Constraint Release in Star/Linear Polymer Blends

M. E. Shivokhin,[†] E. van Ruymbeke,[†] C. Bailly,[†] D. Kouloumasis,[‡] N. Hadjichristidis,[‡,§,#] and A. E. Likhtman*[,⊥]

[†]The Division of Bio- and Soft Matter (BSMA), Institute of Condensed Matter and Nanosciences (IMCN), Université Catholique de Louvain (UCL), Louvain-la-Neuve, Belgium

[‡]Laboratory of Industrial Chemistry, Department of Chemistry, University of Athens, Panepistimiopolis Zografou, 157 71 Athens, Greece

[§]Physical Sciences and Engineering Division, KAUST Catalysis Center (KCC), Polymer Synthesis Laboratory, King Abdullah University of Science and Technology (KAUST), Thuwal 23955-6900, Kingdom of Saudi Arabia

[⊥]School of Mathematical and Physical Sciences, University of Reading, Reading RG6 6AX, U.K.

ABSTRACT: In this paper, we exploit the stochastic slip-spring model to quantitatively predict the stress relaxation dynamics of star/linear blends with well-separated longest relaxation times and we analyze the results to assess the validity limits of the two main models describing the corresponding relaxation mechanisms within the framework of the tube picture (Doi's tube dilation and Viovy's constraint release by Rouse motions of the tube). Our main objective is to understand and model the stress relaxation function of the star component in the blend. To this end, we divide its relaxation function into three zones, each of them corresponding to a different dominating relaxation mechanism. After the initial fast Rouse motions, relaxation of the star is dominated at intermediate times by the "skinny" tube (made by all topological constraints) followed by exploration of the "fat" tube (made by long-lived obstacles only). At longer times, the tube dilation picture provides the right shape for the relaxation of the stars. However, the effect of short linear chains results in time-shift factors that have never been described before. On the basis of the analysis of the different friction coefficients involved in the relaxation of the star chains, we propose an equation predicting these time-shift factors. This allows us to develop an analytical equation combining all relaxation zones, which is verified by comparison with simulation results.

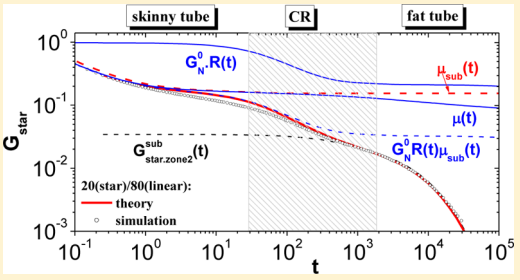

1. INTRODUCTION

The tube theory, initially developed in the 70−80s of the last century[1,2] and continuously refined since, plays a central role in our present understanding of the interrelation between the molecular structure of synthetic polymers and their viscoelastic properties as well as complex flow-behavior. Mathematical models developed based on tube theory have now reached, in many cases, a quantitative level of prediction for the linear rheological characteristics of well-defined molecular structures with narrow distribution of molecular weights.[5,8,13,14] However, understanding the viscoelastic properties of complex molecular architectures, such as those used in industrial applications, still raises many crucial questions arising from the coupling of molecular relaxation mechanisms, in particular, the effect on the relaxation dynamics of a given "probe" chain by relaxing surrounding chains. This effect is partly taken into account by the mechanism called constraint release (CR), which describes the motions of the tube surrounding the probe chain. These motions are due to the relaxation of the surrounding chains and lead to the loss and creation of new entanglements along the probe chain.

In order to gain deep understanding of this process, it is of prime importance to study the dynamics of well-defined model systems. In particular, bidisperse mixtures with well-separated molecular weights, such as binary blends of monodisperse linear chains[16,19−21,38] and star/linear mixtures,[17,23−26] allow us to clearly point out the CR effect of a fast component on the motion of a slow relaxing component.

Understanding CR and its effect on the other relaxation mechanisms in such simplified systems should help us build a general understanding that could be later extended to more complex cases of polydisperse linear and branched polymer mixtures.

Competing theories based on two extreme approaches, i.e., tube dilation[28−30] and tube rearrangement,[1,18,27,31−33,39] have been proposed for describing effects of CR on diffusion and stress relaxation of the slow relaxing chains in binary blends.

The first approach assumes that fast chains, as soon as they have reached their terminal time, act as a solvent for still unrelaxed chains, causing enlargement of the tube diameter. This allows the long (unrelaxed) chains to move in a dilated tube with a diffusion coefficient defined by chain friction only. This approach was applied to predict stress relaxation in polydisperse melts of linear chains,[28] melts of stars,[30] and polymers with more complex branched topologies.[9,10,12]

At the other extreme, the tube rearrangement approach assumes that a long chain is constrained by the so-called skinny tube, which comprises entanglements with short *and* long chains,

Received: December 3, 2013
Revised: March 4, 2014
Published: March 21, 2014

even *after* the relaxation of the short component. However, in addition to the chain motions in the skinny tube, the tube itself can move and explore the fat tube, which only includes entanglements with the other long chains and which constrains the skinny tube. Thus, the long chains are diffusing within the skinny tube while the skinny tube itself is exploring the fat tube by Rouse motion, or by tube reptation motion in the case long chains are mutually entangled. In this picture, the terminal time is determined by a competition between these relaxation mechanisms.[39] In the discussion below we will refer to these two CR pictures as Doi and Viovy theory, respectively.

In their original implementation, both of the above-mentioned theories were tested for predicting the stress relaxation and longest relaxation time of binary linear blends. Numerous published experimental data on binary linear blends have shown dependence of the terminal time on the concentration of the long chains. This observation thus seems to favor the Doi picture. However, it must be mentioned that neither of these two theories accounts for CLF.

D. Read et al., in ref 7, instead follow Viovy but include the influence of CLF. They argue that diffusive motion along skinny tube combined with local CR motion provides enough freedom for CLF to take advantage of the fat tube. This improvement to the original Viovy theory is able to provide an explanation for the long chains concentration dependence of the terminal time.

In order to gain a fundamental insight in the complex interrelated relaxation mechanisms in bidisperse systems, it is useful to compare tube theory predictions with more detailed models. In this respect, the single chain stochastic model, referred to as the slip-spring model,[4] is an interesting candidate since it combines a refined description of molecular dynamics with the ability to predict stress relaxation at long time-scales and allows an overlap with all tube relaxation processes. For maximal discrimination, we test the Doi and Viovy constraint release theories with the help of specially synthesized star/linear blends, characterized by a strong separation between terminal relaxation times of the pure components and a significant level of entanglements.

In order to understand CR in these blends and its contribution to stress relaxation, we first use the slip-spring model as benchmark to correctly predict the individual stress relaxation functions of the star and linear chains, first on their own, then, without any further parameter adjustment, for blends at all compositions. The agreement is found to be quantitative. Next, we reconstruct the stress relaxation function of star chains in the blends and study the relative contribution of each mechanism at different time scales. The slip-spring model allows us to objectively compare the effects of different CR assumptions on the relaxation of the star chains in the blends and assess their validity in different circumstances. Thus, in our study, we simulate and analyze the relaxation of star chains, either in the monodisperse state or blended with linear chains, avoiding direct reliance on CR theories. This objective is in line with the work of Watanabe et al.,[34−37] who are using dielectric spectroscopy measurements of polymers with electrical dipoles aligned along the chain backbone in order to evaluate the time-dependence of the tube survival fraction, $\varphi'(t)$, without relying on any model. By comparing the stress relaxation function, $\mu(t)$, obtained from viscoelastic measurements with $\varphi'(t)$, the authors demonstrate that CR in monodisperse stars predicted by the tube dilation picture cannot be validated. In our paper, the extra information is coming from slip-spring simulations, rather than from dielectric data.

In order to validate our approach, we prepare polymer mixtures of monodisperse star and linear chains, where both components are well entangled and their longest relaxation times are well separated, and measure their linear viscoelastic behavior. This will allow us to validate the slip-spring simulation results as well as to further discuss the role of CR.

This paper is arranged as follows: in the Experimental Section, we describe details of the synthesis and molecular structure of the polybutadiene polymers used in this study. Details of the experimental measurements and data processing are also provided. In the Theoretical Section, we describe a stochastic slip-spring model and its main parameters. In the Results and Discussion, the model is validated by comparison with the experimental data and detailed analysis of the corresponding main relaxation zones (as defined in tube theory) is provided. In the Conclusions, we summarize the key results of this study and propose possible steps toward generalizing the proposed approach to more complex cases.

2. EXPERIMENTAL SECTION

Materials. The synthesis of the linear (M_w = 7.5 kg/mol) and 3-arm star (M_w = 76.0 kg/mol) polybutadienes (PBds) was achieved by anionic polymerization high vacuum techniques. All manipulations were performed, under high vacuum, in home-made glass reactors provided with break-seals for the addition of reagents and constrictions for removal of products. The reactors were previously washed with a benzene solution of *n*-butyllithium (Aldrich) followed by rinsing with benzene, the polymerization solvent. The purification of the monomer butadiene (99%, Aldrich), the solvent benzene (99.8%, Aldrich), the terminating agent methanol (99.9%, Aldrich), and the linking agent $(CH_3)SiCl_3$ (99%, Aldrich) to the standards required for anionic polymerization, was performed according to well-established high-vacuum procedures.[43] *sec*-Butyllithium (*sec*-BuLi), the initiator, was prepared in *vacuo* from *sec*-butyl chloride (99.9%; Aldrich) and a lithium dispersion (99%, high sodium, Aldrich).

SEC experiments were carried out at 25 °C using a Waters Model 510 pump and Waters Model 401 differential refractometer. A four μ-Styragel columns set with a continuous porosity range from 10^5 to 10^1 nm was used. Chloroform was the carrier solvent at a flow rate of 1 mL/min. Polybutadiene standards were used to calibrate the instrument. The microstructure of the dienic precursors was analyzed by ^{1}H NMR (Bruker AC200) spectroscopy in $CDCl_3$ at 30 °C.

The general reactions for the synthesis of the linear and 3-arm star PBds are given in Scheme 1.

Scheme 1. General Reactions for the Synthesis of Linear and 3-Arm Star PBds

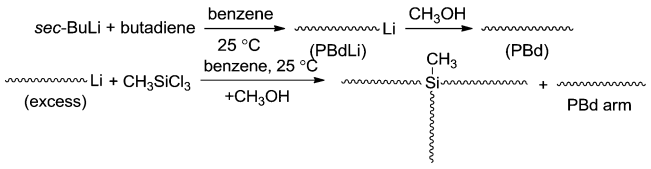

The linear PBd was prepared by polymerization of butadiene with *sec*-Buli as initiator, in benzene at room temperature for 24 h, followed by neutralization with methanol. The SEC trace of the linear PBd is given in Figure 1.

The 3-arm star PBd was prepared by reaction of excess (25%) living PBd with trichlorosilane under the same conditions for

dx.doi.org/10.1021/ma402475a | *Macromolecules* 2014, 47, 2451−2463

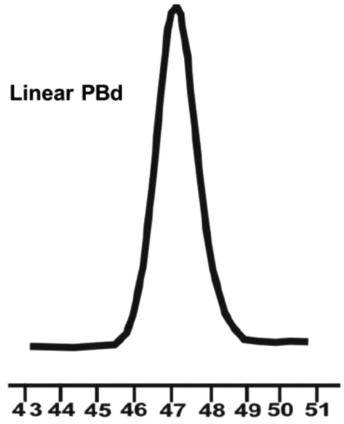

Figure 1. SEC trace of linear PBd.

5 days. Prior to the addition of the coupling agent, a sample of the linear arm was removed and terminated with methanol for characterization. The SEC traces of the arm precursor and the fractionated 3-arm PBd are given in Figure 2.

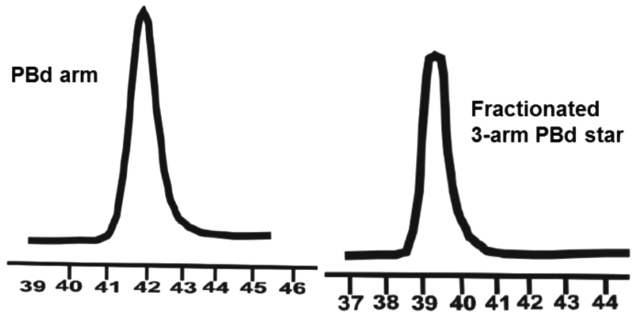

Figure 2. SEC traces of the arm and fractionated 3-arm star PBd.

The star-branched polymer was separated from the unreacted excess of PBd by two consecutive fractional precipitations from a benzene-methanol mixture containing 4-methyl-2,6-di-*tert*-butylphenol as antioxidant (0.02%). The final samples were dried to constant weight and stored under vacuum in the dark.

The molecular weight characteristics of the samples, given in Table 1, show that the synthesized samples are well-defined

Table 1. Molecular Characteristics of the Linear and 3-Arm Star PBd[a]

	linear PBd or arm of the 3-arm star		3-arm star PBd	
sample	M_w (kg/mol)	PDI (M_w/M_n)	M_w (kg/mol)	PDI (M_w/M_n)
linear PBd	7.5	1.02	–	–
star PBd	24.5	1.02	76.0	1.04

[a] M_w and PDI were determined by SEC in THF at 30 °C, calibrated with PBd standards.

with very low polydispersity index (PDI). The microstructure of all samples determined by ^{1}H NMR in CDCl3 was 10% 1,2 and 90% 1,4.

Measurements. For all studied star/linear blends and monodisperse components rheological measurements have been conducted at small deformation to ensure linear response to applied excitation. An ARES (TA Instruments) rheometer was used in oscillatory shear mode with an 8 mm plate–plate fixture. For determining storage, G', and loss modulus, G'', throughout the whole relevant frequency range, time–temperature superposition was used (TTS). The values of storage and loss moduli in the angular frequency range from 0.01 to 100 rad/s were measured at temperatures between 25 and −75 °C (in nitrogen environment) and shifted horizontally toward a reference temperature T_{ref} = 25 °C according to shift factors obtained using WLF equation with parameters C_1 = 4.66, C_2 = 154.33K. We account for influence of different T_g on WLF parameters by introducing an iso-free-volume correction to the shift factors $\log_{10} a_T = -C_1(T - T_{ref} + C_{Tg}/M_w)/(T + C_2 + C_{Tg}/M_w)$, where $C_{Tg}/M_w = (T_g^{inf} - T_g)$ and C_{Tg} = 13 is an empirical Flory–Fox parameter that is related to the free volume for a given polymer chemistry.[41] For taking into account the change of density with temperature, the vertical shift factor

$$b_T = \frac{\rho(T)T}{\rho(T_{ref})T_{ref}} = \frac{(\rho_0 - TC_3 \times 10^{-3})(T + 273.15)}{(\rho_0 - T_{ref}C_3 \times 10^{-3})(T_{ref} + 273.15)}$$

was introduced, with relevant values of the parameters for PBd C_3 = 0.69, and $\rho_0 = \rho(T = 0\ °C)$ = 0.95 g/cm^3.[40] The results are presented in Figure 4.

3. THEORETICAL SECTION

The Slip-Spring Model. The slip-spring model is a single chain bead–spring model describing dynamics of entangled polymers. The main distinctive feature of the slip-spring model resides in the way interactions with surrounding chains are implemented. Effects from entanglements are modeled via slip-links along the chain. Each slip-link is connected with its anchored end via a virtual spring with parabolic potential (see Figure 3). All implementation details of this model can be found in reference.[4]

The total potential energy of the chain in this model is calculated by summing up potential energy of the chain itself (springs connecting each couple of beads) and the total potential energy of virtual springs representing the effect of entanglements. These slip-links are randomly distributed along the chain. The distribution of anchoring points is chosen from conditions that the slip-springs must not perturb Gaussian statistics of the chain over all length scales.

The disentanglement and re-entanglement process is modeled by tracing a binary correspondence between every couple of chains forming each entanglement. When a chain-end diffuses through an entanglement, the corresponding slip-link disappears simultaneously from two chains and a new slip-link associated with a new arbitrary partner of the probe chain is created at random position along the chain. It must be noted that the model assumes that all entanglements are binary and therefore the dilution exponent, α, is considered as equal to 1 in this work:[42] any chain end diffusing out of a slip-link leads to the disentanglement of exactly two chains. We also introduce an effective repulsion between slip-links, which prevents two neighboring slip-links from crossing each other and be closer than two beads apart; this makes chains effectively more entangled, as compared to the case without repulsion.

The slip-spring simulation results are presented in dimensionless units, with thermal energy k_BT = 1, size of the Kuhn segment, b = 1 and effective friction coefficient of a Kuhn segment, ζ = 1. The stress relaxation function is calculated from the Green–Kubo relationship, including chain stress autocorrelation and the cross-correlation between the chain stress and the stress carried out by the virtual springs.[6,46]

dx.doi.org/10.1021/ma402475a | *Macromolecules* 2014, 47, 2451–2463

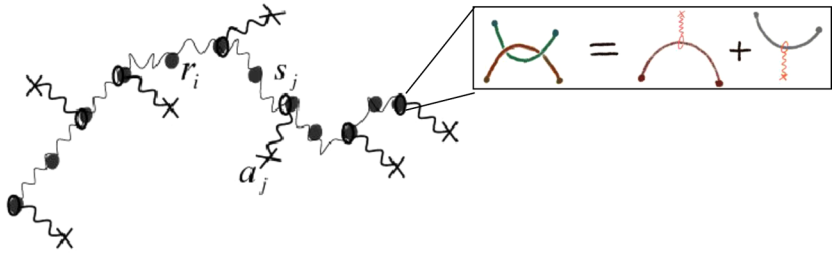

Figure 3. Schematic representation of a slip-spring model (adopted from refs 4 and 6).

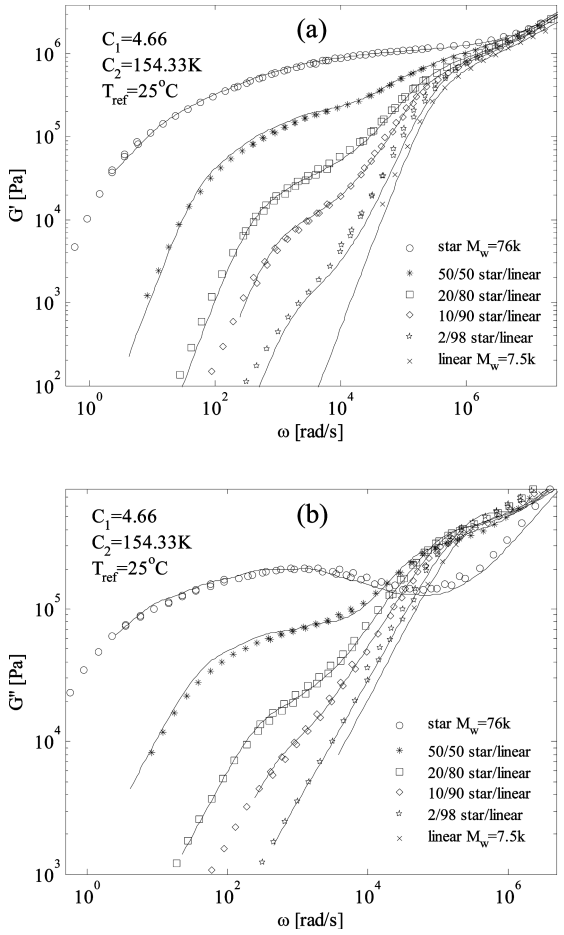

Figure 4. Simulation results of the slip-spring model superimposed with (a) the experimental dynamical storage and (b) loss moduli of binary polymer mixtures of symmetric star M_w = 76 kg/mol and linear chains M_w = 7.5 kg/mol. Concentration of components varies from 100% of stars (upper curve) to 100% of linear chains (lower curve). Simulations results and experimental data are indicated with solid lines and markers, respectively.

Before simulating stress relaxation of the blends, we first calibrate the material parameters used in the model by fitting predicted stress relaxation curves to the experimental data for the same monodisperse star and linear polymers as used in the blends. Next, we use the same values of the material parameters for simulating the viscoelastic properties of the blends at all concentrations.

Regardless of molecular topology and molecular weight, we use N_e = 4 as average number of beads between two slip-links, N_s = 0.5 as virtual spring strength, and a unit discrete slip-link jump of size 1 at every time step dt = 0.05 in a Metropolis Monte Carlo simulation. The slip-links are further not allowed to cross the branch point.

For mapping the length-scale of the model to the experimental data, we fit the molecular weight represented by one bead as M_0 = 0.34 kg/mol. For mapping the simulated time-scale and stress to the experiment, we multiply the dimensionless values by $\tau_0(T = 25\ ^\circ\mathrm{C}) = 5.13 \times 10^{-6}$s and G_0 = 7.5 MPa, respectively. We note here that the stress of the model is calculated in units of $G_0=\rho RT/M_0$ with ρ, R and T being the polymer density, universal gas constant and absolute temperature, respectively. G_0 should not be confused with the plateau modulus G_N^0.

4. RESULTS AND DISCUSSION

4.1. Predicted Viscoelastic Data Based on the Slip-Spring Model. In Figure 4, the storage and loss moduli predicted by the slip-spring model are compared to the experimental data for the different mixtures of symmetric star and linear chains. A very good agreement is obtained, whatever the proportion of star chains in the blend. In particular, the level of the second plateau, which appears at low frequency in the storage modulus, is well predicted despite the fact that, in the model, entanglements are always considered as binary events. This corresponds, in the tube picture, to a dynamic dilution exponent, α, equal to 1.[42] Furthermore, one can also observe a good match between experimental and predicted curves in the transition zone localized between the relaxation of the linear and star chains. Understanding the mechanisms dominating this zone is particularly interesting since most tube-based approaches fail to correctly capture the viscoelastic curves in this region, as they show too abrupt decrease of the storage modulus.

To our knowledge, this is first time that predictions of the stress relaxation by the slip-spring model are presented for pure stars. Despite the fact that the focus of this paper is not on pure stars, this is of great significance to validate the slip-spring model by confronting its predictions with published data for "nearly monodisperse" stars with different molecular weights (see also appendix B).

The slip-spring model can hence be used as a benchmark for predicting the viscoelastic behavior of star-linear blends. It is interesting to further analyze these results and map them to the relaxation mechanisms identified in tube theory (such as arm retraction and constraint release). Indeed, as discussed in the introduction, many questions are still open today in tube theory, such as, for example, how to account for the influence of the fast relaxing component (which are the linear chains in our case) on the relaxation of the slow component (the star chains in our case). Do these slow components relax in a skinny tube or a fat tube? Decomposing the slip-spring data into these different contributions should help us addressing these questions.

To do so, since the relaxation of the linear chains is relatively well understood, we focus only on the relaxation function of the

dx.doi.org/10.1021/ma402475a | Macromolecules 2014, 47, 2451−2463

star chains, $G_{star}(t)$. We propose to divide the stress relaxation function predicted by the slip-spring model into three main relaxation zones and to analyze the different relaxation mechanisms, which are active in each of them. As illustrated in Figure 5 for the 20/80 star/linear blend, the three zones

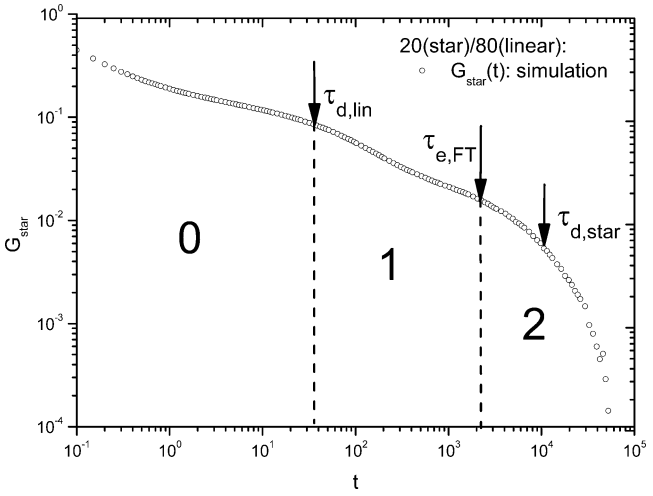

Figure 5. Slip-spring prediction of stress relaxation function of star components in the 20/80 star/linear blend. Arrows show reptation time of the linear components, $\tau_{d,lin}$, constraint release Rouse equilibration time along span of two star arms, $\tau_{e,FT}$, and terminal time of the star components, $\tau_{d,star}$. The arrows represent virtual separation on characteristic relaxation zones according to dominant relaxation mechanisms: (0) fast Rouse relaxation modes at $t < \tau_{d,lin}$; (1) Rouse constraint release zone at $\tau_{d,lin} < t < \tau_{e,FT}$; (2) fat tube zone at $t > \tau_{e,FT}$.

correspond to (i) the relaxation of the star molecules before reptation of the fast linear chains (zone 0), (ii) the relaxation of the star chains just after the reptation of these linear chains, when the star molecules are expected to relax by constraint release (zone 1), and (iii) the terminal relaxation of the slow relaxing star chains (zone 2).

The relaxation mechanism in zone 0 is well-defined: in this region, the chains mainly relax by fast Rouse and arm retraction relaxation modes. Since the times considered are shorter than the relaxation time of the fast relaxing linear chains, we can consider that all initial entanglements are still present and therefore the chains are still confined in their original skinny tube, which corresponds to the equilibrium molecular weight between entanglements, $M_{e,0}$.

Contrary to zone 0, the main relaxation mechanisms in zones 1 and 2 need to be further investigated. To do so, we propose to analyze these two zones separately with the help of slip-spring simulations for different binary star/linear blends presented in this work. In particular, by comparing simulation results obtained for actual star/linear blends to the predictions obtained by considering the same star chains, in same proportion, but relaxing either in a fixed network (which corresponds to a "skinny tube" approach) or in a virtual solvent (which corresponds to a "fat tube" approach), we should be able to analyze the influence of the fast relaxing linear chains on the motion of the star molecules. In order to combine these two relaxation zones, we will then propose a mixing rule (see section 4.4). In such a way, an analytical expression for the stress relaxation will be obtained, which can be used to describe the relaxation of the star component in star/linear blends of different concentrations at any time scale.

4.2. Relaxation of the Star Chains in Zone 1. As mentioned in section 4.1, zone 1 starts just after the reptation of the fast relaxing linear chains. We therefore expect to observe in this area the consequence of the relaxation of these linear chains on the motion of the star molecules. Indeed, the star/linear entanglements can now disappear and appear again somewhere else along the star arms, at the rhythm of the linear chains motions. This blinking feature of the star/linear entanglements allows the star chains to move, even if at this time scale, the star/star entanglements can still be considered as permanent.

The corresponding motions of the star chains are usually described by the constraint release Rouse process (CRR), which considers Rouse-like motions of the skinny tube (including both star/linear and star/star entanglements) in the fat tube, which only accounts for star/star entanglements. In order to determine this fat tube, all the star/star entanglements should be considered as permanent.

Thus, the longest time for equilibration of the skinny tube, with diameter a and number of tube segments n, can be determined from the Rouse reorientation time:

$$\tau_{CRR} = \frac{\zeta n^2 a^2}{3\pi^2 k_B T}$$

with ζ the effective friction coefficient per single bead. The effective friction coefficient can be calculated in the one-dimensional case as

$$\zeta = \frac{k_B T}{D} = \frac{2\tau_{CR} k_B T}{(A_{CR} b)^2}$$

where k_B is the Boltzmann constant, τ_{CR} is the time for a single CR hop, b is the size of the Kuhn segment, A_{CR} is an unknown prefactor and $(A_{CR}b)^2$ is a hop amplitude. We expect $A_{CR}b$ to be on the order of the tube diameter. In section 4.5, we will determine the value of this prefactor.

We can now calculate the necessary time to fully equilibrate n skinny tube segments per single fat tube segment. If the fat tube does not exist due to a very low concentration of the star chains then $n = 2Z_{arm}$, where Z_{arm} is a number of entanglements per star arm. On the contrary, for higher concentrations of stars, we have $n = Z_{arm}/(Z_{arm}\phi_{star}) = 1/\phi_{star}$. Now we can determine the time required for the full equilibration of a single fat tube segment including n skinny tube segments as[7,11,32,33]

$$\tau_{e,FT} = \frac{2}{3\pi^2}\tau_{CR} n^2 \quad (3)$$

We assume that all entanglements between stars and linear chains are released at same frequency $1/\tau_{CR}$, where τ_{CR} is the longest relaxation time of the linear chains in the star/linear blends. This is realized in the simulation by deleting each slip-spring at every step with a probability dt/τ_{CR}, where dt is the time step of the simulation. In our theoretical calculations, we use $\tau_{CR} = \tau_{d,lin} = 60$ (in the model dimensionless time units) for every blend composition. This value is an average (with precision of ±15%, depending on the fraction of the star chains in the blends) for the longest relaxation times obtained from simulated end-to-end vector autocorrelation functions of the linear chains.

In this expression we do not account for the difference between effective CR hop distance, $A_{CR}b$, and tube diameter, a.

The expression (eq 3) is valid only in the range $\tau_{d,lin} < \tau_{e,FT} < \tau_{d,star}$.

It must be noted that $\tau_{e,FT}$, which represents the longest CRR relaxation mode of a single fat tube segment and thus does not

dx.doi.org/10.1021/ma402475a | Macromolecules 2014, 47, 2451−2463

depend on the arm length, also defines the transition between zone 1 and zone 2 (see Figure 5).

On the other hand, although in zone 1, the relaxation of the star chains is dominated by CRR, their arms can also partially relax via a retraction mechanism. Since in this zone, equilibration of the chains in their fat tube is not complete, we assume that this retraction process is constrained by all entanglements, with other star chains as well as with linear molecules. This assumption, which will be validated below, is equivalent to considering the star chain motion within a skinny tube. On this basis, we can determine $\mu(t)$, the average fraction of initial tube segments which are still oriented at time t, as equal to the predicted stress relaxation function of the star chain in a permanent network. This is shown in Figure 6 by blue diamonds.

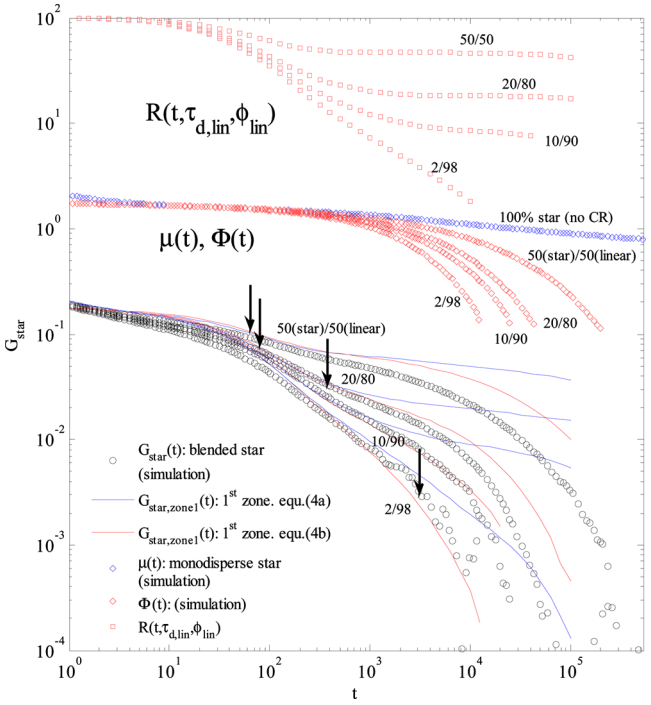

Figure 6. Simulation results: In the lower part of the plot we show comparison between the star stress relaxation function obtained by simulating the motion of the full blends (circles), and the stress relaxation function obtained based on eqs 4a, blue solid curves, and 4b, red solid curves. The relaxation function of the star component in the skinny tube, $\mu(t)$, obtained by running slip-spring simulations of the monodisperse star with deactivated CR is shown (blue diamonds) in the central part of the plot. The end-to-end vector autocorrelation functions of the star component at every blend composition, $\Phi(t)$, are shown by red diamonds. Red squares in the upper part of the plot show tube relaxation function, $R(t,\tau_{d,lin},\phi_{lin})$, dominated by balance between CR skinny tube motion and stress equilibration of the chain by Rouse process. Different ratios of star/linear components from 50/50 to 2/98 have been considered. Solid arrows represent transition between zone 1 and zone 2 (eq 3). $\Phi(t)$, $\mu(t)$, and $R(t,\tau_{d,lin},\phi_{lin})$ curves were freely vertically shifted for better visual representation.

However, the CR process can also speed up the relaxation of the chain inside the skinny tube. To check this we compute the end-to-end vector autocorrelation function of the star chains, $\Phi(t)$, for every blend composition, and compare it with $\mu(t)$ computed from pure star simulations (see eq 4b and plotted by red diamonds in Figure 6).

Retraction and CRR processes must next be combined for determining the stress relaxation function of the star chains, $G_{star,zone1}(t)$, in a star/linear blend. To do so, we follow the idea of Graessley,[18] assuming independence between the chain motions inside the skinny tube and the Rouse-like dynamics of this skinny tube itself inside the fat tube:

$$G_{star,zone1}(t) = \mu(t)R(t, \tau_{d,lin}, \phi_{lin})G_N^0 \quad (4a)$$

$$G_{star,zone1}(t) = \Phi(t)R(t, \tau_{d,lin}, \phi_{lin})G_N^0 \quad (4b)$$

where $R(t,\tau_{d,lin},\phi_{lin})$ is the skinny tube relaxation function of the star chains in the blends due to CR. This function is obtained by running a slip-spring simulation with all star/linear entanglements "blinking" with the same frequency, $1/\tau_{d,lin}$, and star/star entanglements having infinite relaxation time, τ_{inf}. Besides that, escape of chain ends from slip-links representing entanglements with other chains is prohibited. This condition is equivalent to neglecting contribution to relaxation by escape of the chain from the tube by arm retraction or reptation. The so obtained function R includes combined relaxation contributions from CR motion of the skinny tube and Rouse stress equilibration of the chain. Morever we prohibit slip of entanglements along the backbone, thus we do not account in $R(t,\tau_{d,lin},\phi_{lin})$ for the longitudinal Rouse relaxation modes, which are not active.

For calculation of $R(t,\tau_{d,lin},\phi_{lin})$, all Rouse relaxation modes faster than entanglement equilibration time, τ_e, have been subtracted in order to avoid double counting of these modes with those accounted for in $\mu(t)$ or $\Phi(t)$ in zone 0. Details of the mode subtraction procedure will be discussed in section 4.4. For simplicity, in the following discussion we will refer to this newly introduced function, $R(t,\tau_{d,lin},\phi_{lin})$, as the tube relaxation function. The function $R(t,\tau_{d,lin},\phi_{lin})$ is normalized such that $R(0) = 1$.

In eqs 4a and 4b, we introduce a prefactor G_N^0, which ensures that in the absence of relaxation $\mu = 1$, $R = 1$ and no longitudinal relaxation the resulting stress level is equal to the plateau modulus.

In Appendix A, we compare the time dependence of the newly proposed function $R(t,\tau_{d,lin},\phi_{lin})$ with another function traditionally used for modeling tube relaxation in bidisperse blends. This function is obtained by simulating the Rouse dynamics of an unentangled star chain containing "slow" and "fast" beads.[15]

Once all necessary parameters have been defined, the relaxation function $G_{star,zone1}(t)$ of the star component in the different star/linear blends can now be determined, based on eqs 4a or 4b. Comparison between these curves and the relaxation function predicted by direct simulation of the blend relaxation (as presented in Figure 2) is shown in Figure 6:

All predictions by eqs 4a and 4b, shown by solid red and blue curves in the lower part of Figure 6 demonstrate systematic deviations at $t = \tau_{d,lin}$ (shown with a solid arrow for a 50(star)/50(linear) blend). This can be attributed to the simplified relaxation spectrum of the linear chains used in the calculations. In our calculations we only account for their longest relaxation time, whereas moderately entangled linear chains have much broader distribution of possible relaxation times, including chain fluctuations and reptation modes. However, we allow this simplification as the major part of the chain is still relaxing by reptation.

We find that in zone 1, limited by solid arrows, the agreement between both methods and full simulation is very good for the blends containing at least 10 wt % of star chains. That means that in this region and for ϕ_{star} = 10 wt % the star relaxation is not influenced by CR from the linear chains.

dx.doi.org/10.1021/ma402475a | Macromolecules 2014, 47, 2451−2463

By contrast, for the blend with the lowest star concentration (2 wt %), the CR contribution from linear chains does contribute significantly to the star relaxation. This is validated by the fact that theoretical predictions shown by solid red and blue curves deviate from each other in the time-scale limited by the arrows. Thus, for best fitting of the total stress relaxation function, $G_{star}(t)$ for the lowest star concentration we have to use eq 4b, with concentration dependent star relaxation function, $\Phi(t)$. At this blend composition, the concentration of star chains is very low: $N_{arm}\phi_{star}/N_e < 1$. Therefore, the fat tube does not exist and the star chain relaxation is terminated by CRR motion in zone 1. This blend is the exception from the general rule which we can draw for the other blend compositions. Namely, before the full equilibration of the star chains by CRR ($t < \tau_{e,FT}$), the retraction mechanism of the star chains takes place in the skinny tube, which, itself, is moving in a fat tube, similarly to a Rouse chain containing beads with different lifetimes. Further, these two relaxation processes are independent.

We should also note that the solid arrows showing the CR equilibration time of the skinny tube inside the fat tube segment ($\tau_{e,FT}$, end of zone 1) often do not coincide with the onset of deviations between $G_{star,zone1}(t)$ (solid lines in Figure 6 corresponding to eq 4) and $G_{star}(t)$ (slip-spring predictions shown by black circles). That could be ascribed to the existence of some transition zone which is still strongly affected by the linear chains even after the fat tube has already been explored.

At longer times, the predictions of eqs 4a and 4b, strongly deviate from the results obtained by the simulation of the star/linear blends at all compositions except for the blend with 2 wt % of star chains. As discussed in the next section, this is most probably due to the fact that arm retraction does not happen in the skinny tube at that time scale.

4.3. Relaxation of the Star Chains in Zone 2. In this section, we discuss relaxation of the star chains at times larger than fat tube CR-equilibration time. In this time zone, the star chains are assumed to move in the fat tube created by the star/star entanglements. As already mentioned, two main ideas can be followed: the first one[28] considers that the linear chains act as a solvent. The star/linear entanglements can then simply be ignored and the effective molecular weight between two entanglements is considered as equal to $M_{e,0}/\phi^{\alpha}_{star}$, where $\alpha = 1$.[42] On the other hand, according to the second idea,[39] the star chains stay constrained by the skinny tube even after its complete CR-equilibration in the fat tube.

As shown in Figure 6 (solid lines), if we consider that the arm retraction of star chains happens in the skinny tube, the predicted star relaxation function is far too slow compared to the reference results of the slip-spring simulations. Since we consider that in this time zone, arm retraction is the only possible relaxation process (CR-equilibration has reached the limit of the fat tube), this picture cannot be validated here.

Next, we test the idea proposed by Doi, according to which the arm retraction in zone 2 takes place in the fat tube. To do so, the results obtained by simulating the motions of the star/linear blends are compared to the results obtained by simulating the relaxation of truly diluted monodisperse star chains containing the same average number of star/star entanglements as the star chains in the star/linear blend, i.e. $M_{e,\text{"diluted star"}} = M_{e,0}/\phi_{star}$. According to Doi's picture, these two curves should be identical in time zone 2.

In Figure 7, we plot the pure contribution from star/star entanglements to the total stress relaxation function, $G^{sub}_{star,zone2}(t)$, after having subtracted the fast Rouse modes of the "diluted" star as

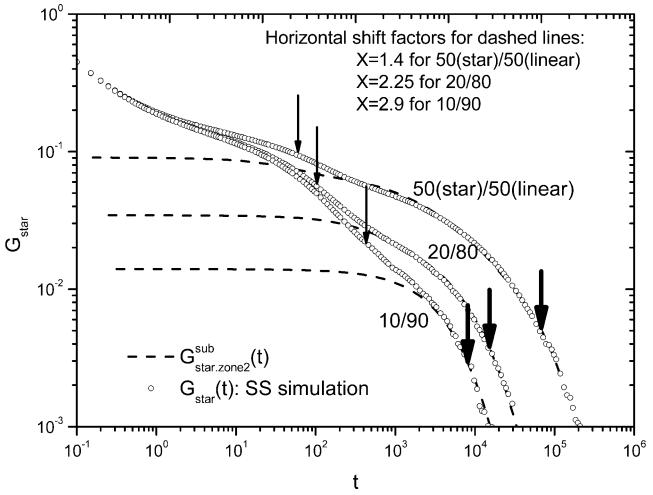

Figure 7. Comparison between the simulated star relaxation function in the star/linear blends and horizontally shifted relaxation function of "diluted" monodisperse star containing the same average number of star/star entanglements and having subtracted fast Rouse relaxation modes, $G^{sub}_{star,zone2}(t)$. The results are shown for all studied star/linear compositions, having fat tube zone (from 50(star)/50(linear) to 10/90). Thin arrows highlight the transition between zone 1 and zone 2 (see Figure 5). The thick arrows highlight the longest relaxation time of the star component.

in zone 1. Further details about subtracting the fast Rouse modes will be discussed in section 4.4. While the *shape* of the relaxation function of the diluted monodisperse star chains correctly fits the star relaxation function, a quantitative overlap between these curves, which is shown in Figure 7, is only obtained after a horizontal shift of this diluted star data toward longer times. These shift factors, which are discussed below, are due to the fact that in the star/linear blends the motions of the star chains are directly depending on the "blinking" motions of the linear chains and thus on their reptation time. Therefore, the probe chain cannot move freely inside the fat tube in the same way as it moves in a true solvent. Instead, the chain sometimes has to wait for the fast entanglements to disappear. In other words, the effective friction inside the fat tube will depend on the reptation time of short linear chains. Understanding the value of these shift factors is thus of prime importance, in order to get a quantitative picture of the relaxation mechanisms.

These shift factors, $X(\phi_{star})$, have been determined from the condition that the shifted relaxation functions of the "diluted" monodisperse star chains, $G_{star,zone2}(t)$, match well with the simulation results of the star/linear blends:

$$G_{star,zone2}(t) = G_{star}\left(tX(\phi_{star}), \frac{M_{e,0}}{\phi_{star}}\right) \quad (6)$$

They will be analyzed in details in section 4.5.

Based on Figure 7, we observe that a good agreement between the simulation results for the star/linear blends and for the "diluted" monodisperse star chains does not start at the same time for different blends, and seems to depend on their composition.

It must also be noted that according to Doi, zone 2 must be completely dominated by the relaxation of the star component in the dilated tube. Therefore, in order to validate this picture, the gap between thin and thick arrows in Figure 7, corresponding to the time scale of zone 2, should completely overlap with the

dx.doi.org/10.1021/ma402475a | Macromolecules 2014, 47, 2451−2463

dashed lines representing the star component contribution, which is not the case. Besides, Doi's original picture does not allow for a horizontal shift of the relaxation curves, and hence, clearly overestimates the dilation effect on the longest relaxation time of the star, especially at low star concentration.

On the other hand, we can observe that, at high star concentrations, a good overlap is obtained over a wide time window because the actual star relaxation function, $G_{star}(t)$, is completely dominated by the slow modes correctly described by the tube dilation approximation, $G_{star,zone2}(t)$,when allowing for a suitable time-shift.

By contrast, at lower values of ϕ_{star}, complete match can be observed only at much longer times near the terminal zone.

By comparing Figure 6 and Figure 7 we can conclude that the effect of the linear chains is dominating star relaxation well beyond zone 1, whereas the tube dilation picture can be validated for blends with star chains concentration of at least 10 wt %, if one accounts for the shift factors.

4.4. Mixing Rule for First and Second Relaxation Zones. In this section, we propose a mixing rule, in order to merge the relaxation behavior observed in zone 1 (section 4.2) and zone 2 (section 4.3) into a single equation, assuming that we know the shift factors $X(\phi_{star})$, which will be discussed in section 4.5.

As concluded in section 4.3, the relaxation in zone 2 of a star probe chain in a star/linear blend can be modeled by the shifted relaxation function of the equivalent diluted monodisperse star component, $G_{star,zone2}(t)$. In order to be able to also use this relaxation function in zone 1, it is necessary to remove the contribution of the fast Rouse relaxation modes.

First, we fit $G_{star,zone2}(t)$ using a Prony series for the shear relaxation modulus $G_{star,zone2}(t) = \Sigma_{i=1}^{N} G_i \exp(-t/\tau_i)$ where G_i and τ_i are moduli and relaxation times of the Maxwell modes. All those modes which are faster than entanglement Rouse equilibration time, defined as $\tau_e=\tau_{e,0}/\phi_{star}^2$ where $\tau_{e,0}$ is the entanglement equilibration time in undiluted case, are next subtracted. Obtained in this way, $G^{sub}_{star,zone2}(t)$ for every blend composition is constant at time scale of $t < \tau_e$, as shown in Figure 7.

As discussed in sections 4.2 and 4.3, relaxation zones 1 and 2 can be modeled by considering only the corresponding dominant relaxation mechanism. It does not imply that relaxations by other involved mechanisms are frozen, however their effect is hidden by the dominant relaxation. Here, we would like to consider an expression for the total stress relaxation function, $G_{total}(t)$, which accounts for all these relaxation mechanisms, even if they are negligible in certain time zones. This will ensure the validity of $G_{total}(t)$ at every time. To this end, since in the case considered here the relaxation of the linear chains and of the star chains are well-separated, we use a multiplicative mixing rule, which is based on the assumption of independence between relaxation mechanisms dominating zones 1 and 2:[15,18]

$$G_{total}(t, \phi_{star}) = G_N^0 R(t, \tau_{d,lin}, \phi_{lin}) \mu_{sub}(t) \frac{G^{sub}_{star,zone2}(t)}{G^{sub}_{star,zone2}(0)} \quad (8)$$

In this expression, $R(t,\tau_{d,lin},\phi_{lin})$ is the skinny tube relaxation function defined in section 4.2, including the subtraction of fast Rouse modes. The term $\mu_{sub}(t)$ represents the orientation survival function of the probe chain obtained by slip-spring simulations and plotted as blue diamonds in Figure 6, from which modes slower than $\tau_{e,FT}$ have been subtracted. The product $R(t,\tau_{d,lin},\phi_{lin})\mu_{sub}(t)$ hence represents the dominating relaxation in zone 1. $G^{sub}_{star,zone2}(t)$ is the stress relaxation function of a diluted monodisperse star after subtraction of the fast Rouse modes and accounting for time-shift factor, $X(\phi_{star})$ described in section 4.5. It thus represents the dominating relaxation in zone 2. The prefactor $1/G^{sub}_{star.zone2}(0) \sim 1/\phi_{star}$ is introduced for normalizing contributions from both relaxation mechanisms. Indeed, in zone 1, $R(t,\tau_{d,lin},\phi_{lin})$ is dominating G_{total}, and $G_{star,zone2}(t) \sim \phi_{star}$ is constant whereas, in zone 2, $G_{star,zone2}(t)$ is dominating the total relaxation function and $R(t,\tau_{d,lin},\phi_{lin})$ is constant $\sim\phi_{star}$.

As shown in Figure 8, a good agreement is obtained between the simulation results for the star/linear blends and the

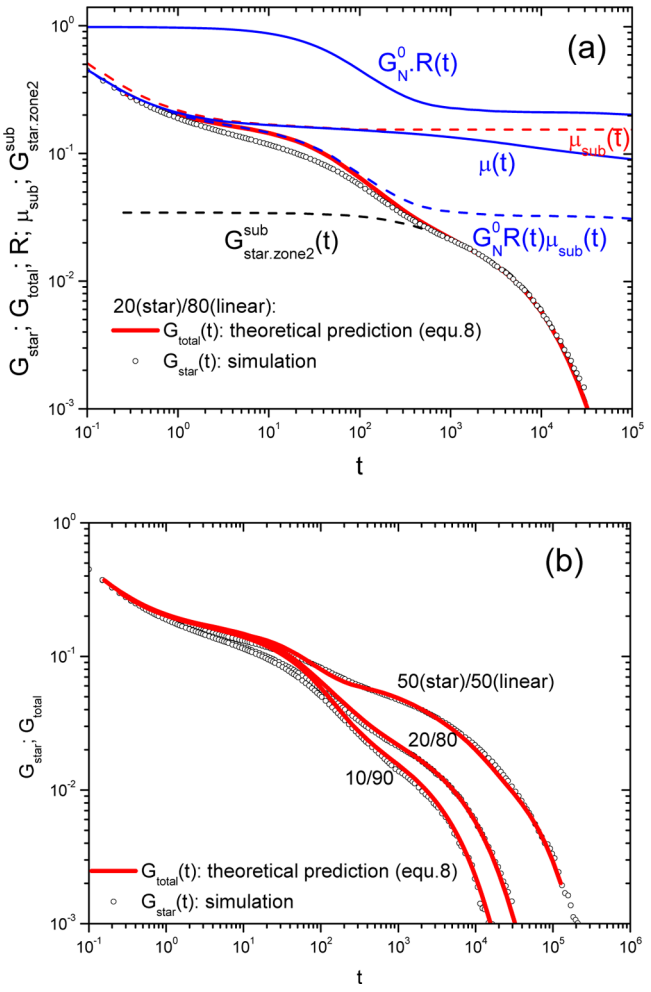

Figure 8. (a) Simulation results of the star relaxation in single blend composition with 20 wt % of the star chains; all components of eq 8 including total star relaxation function $G_{total}(t)$ (red solid line) superimposed with the corresponding simulation data (black circles). (b) Simulation results superimposed with the theoretical predictions. Total relaxation function of star component in the star/linear blend determined by merging two characteristic relaxation zones using eq 8 (red solid lines), superimposed with prediction by slip-spring model (black circles). Different ratios of star/linear components from 50/50 to 10/98 are presented from up to down.

predictions based on the mixing rule (eq 8). The stress relaxation function of the star component in blend 2/98 is not shown in Figure 8, because it is completely predicted by eq 4b, describing stress relaxation in zone 1 (see Figure 6).

We therefore have all necessary ingredients to predict the star relaxation in star/linear blends from separate simulations apart

dx.doi.org/10.1021/ma402475a | Macromolecules 2014, 47, 2451−2463

from the time shift factors $X(\phi_{star})$, which we compute in the next section.

4.5. Effective Friction in the Fat Tube. From comparison of the terminal zone relaxation with the simulation of pure diluted stars (Figure 7), we have seen that the shape of the relaxation agrees very well, but the full simulation results are shifted toward longer times by a significant factor. This can be explained by noticing that the effective friction of the chain inside the fat tube is larger than the bare friction of the free chain. The reason is quite obvious: the chain can not move freely in the fat tube because it is still constrained by the skinny tube, or by the entanglements with the short linear chains. Ignoring these fast entanglements, as was done in our diluted simulations, will clearly lead to faster relaxation. This is the effect which was overlooked in the tube dilution theory of Ball–McLeish[30] and Milner–McLeish,[22] who assumed that the friction in the fat tube is the same as the friction of the bare chain.

The quantitative theory to predict effective friction in the fat tube was recently developed by D. J. Read et al.[7] It considers two main modes of motion of the chain inside the fat tube. The first is straightforward reptation in the skinny tube, which obviously results in the chain escaping from the fat tube as well. The second mode is reptation in the fat tube due to CR of the short chains.

The friction associated with the first mode ζ_{eff} is independent of CR rate, and the friction associated with the second one is directly proportional to CR rate. One can assume that these two contributions are independent, and therefore the total friction in the fat tube is given by

$$\frac{1}{\zeta_{tot}} = \frac{1}{\zeta_{CR}^{tot}} + \frac{1}{\zeta_{eff}} \tag{9}$$

For clarity, for all mechanisms, we shall compute the total friction of the whole chain, i.e., the center of mass friction. Since all relaxation mechanisms discussed here are local, the center of mass friction is $N\zeta^{mon}$, where ζ^{mon} is the corresponding friction per monomer.

According to the pure reptation theory of Doi and Edwards, the reptation time is given by $\tau_d = (L^2\zeta_0^{cm})/(\pi^2 k_B T)$, where ζ_o^{cm} is the friction coefficient of the whole chain in the skinny tube. If the only relaxation mode in a fat tube is reptation in the skinny tube, the reptation times in both tubes must be the same. This has to be the case because at the moment the chain escapes from the skinny tube, it escapes from the fat tube as well. By equating these two reptation times, we get

$$\tau_d^{fat} = \tau_d^{skinny} \rightarrow L_{fat}{}^2\zeta_{eff} = L_{skinny}{}^2\zeta_0^{cm}$$

We know that the fat tube is shorter than the skinny tube, therefore the friction in the fat tube must be larger to produce the same reptation time. More precisely, since the tube length is equal to

$$L = \frac{Nb^2}{a} = \frac{Nb}{\sqrt{N_e}}$$

and N_e changes with concentration as $N_e = N_e^{melt}/\phi_{star}$, the ratio of the skinny and fat tube lengths squared must be

$$\left(\frac{L_{fat}}{L_{skinny}}\right)^2 = \phi_{star}$$

which means that

$$\zeta_{eff} = \frac{\zeta_0^{cm}}{\phi_{star}} \tag{10}$$

This is a central result of ref 11, which is also manifested by the fact that the corresponding Rouse time in the fat tube is larger than the bare Rouse time by a factor of $1/\phi_{star}$.

We plot the predictions of eq 10 in Figure 10 (dashed line) and compare them with the shift factors we determined empirically (circles and squares). According to eq 9, our simple eq 10 is an upper estimate for the friction.

Indeed, the empirical shift factors lie below this simple prediction, because CR reduces the total friction. To estimate this friction ζ_{CR} independently, we run separate simulations of the star Rouse chain with slip-springs which do not slip along the chain (and thus never escape from the tube), but appear and disappear with constant rate given by $1/\tau_{CR}$ (this simulation model is described in section 4.2). Therefore, the chain dynamics at long time scales is solely determined by slip-springs and their creation/destruction rate. We next use two methods to extract an effective friction of the chain center of mass due to CR. The first is to measure the center of mass mean square displacement of the chain at long times. We get

$$\zeta_{CR}^{MSD} = \frac{k_B T}{\lim_{t\to\infty} g_3(t)/(6t)} \tag{11}$$

where $g_3(t) = \langle (R_{cm}(\tau + t) - R_{cm}(\tau))^2 \rangle$ is the center of mass mean square displacement. Another method is to assume that at long length scales the CR dynamics obeys the Rouse theory, and therefore CR friction can be extracted from the terminal time of the end-to-end relaxation τ_Φ using Rouse expression for a star polymer

$$\tau_\Phi = \frac{(2N_{arm})^2\zeta_{mon}b^2}{3\pi^2 k_B T}$$

where $\zeta_{mon} = \zeta_{CR}{}^\Phi/(N_{arm}M)$ is the friction per monomer, M is the number of star arms, and N_{arm} is the star arm length.

This gives

$$\zeta_{CR}^\Phi = \tau_\Phi \frac{3\pi^2 k_B T}{4N_{arm}b^2} M \tag{12}$$

We perform simulations of this model for the 3-arm star polymer with $N_{arm} = 75$ for a wide range of constraint release times τ_{CR}, and extract CR friction from eqs 11, 12. The results are plotted in Figure 9.

Two limiting cases are apparent. In the limit of $\tau_{CR} \rightarrow 0$, the friction obviously reduces to the bare friction of the chain, $\zeta_{CR} \rightarrow \zeta_0^{cm}$. In the opposite limit $\tau_{CR} \rightarrow \infty$, it is clear that the effective friction must become directly proportional to τ_{CR}. A simple model of a particle hopping a constant distance d at every time interval τ_{hop} leads to the following effective friction

$$\zeta_{hop} = \frac{2\tau_{hop}k_B T}{d^2} \tag{13}$$

By analogy, we expect

$$\frac{\zeta_{CR}}{N_{arm}M} = \frac{2\tau_{CR}k_B T}{(A_{CR}b)^2}, \quad \text{as } \tau_{CR} \rightarrow \infty$$

where A_{CR} is an unknown prefactor with a clear physical meaning: $A_{CR}b$ is an effective monomer hopping distance during

dx.doi.org/10.1021/ma402475a | Macromolecules 2014, 47, 2451–2463

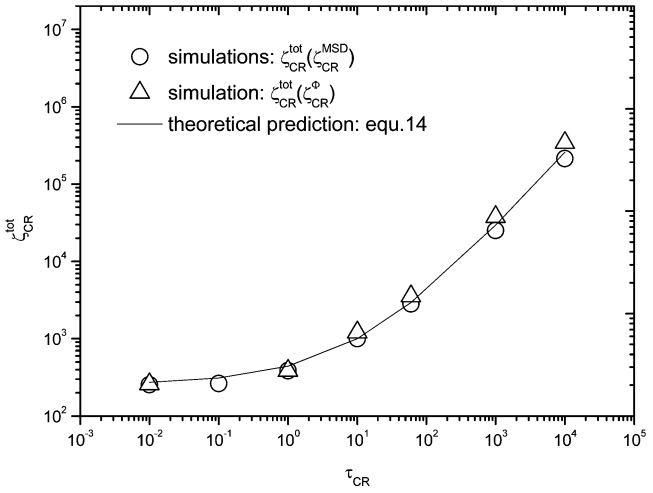

Figure 9. Total CR friction coefficient of star chain, ζ_{CR}^{tot}, obtained by simulating rouse chain with slip-springs not allowed to slip along the chain but appearing and disappearing with constant frequency $1/\tau_{CR}$. Triangles: ζ_{CR}^{tot} obtained from measuring mean square displacement of the center of mass of the star chain at long time scales. Circles: ζ_{CR}^{tot} extracted from the terminal times of the end-to-end vector relaxation. Solid line: theoretical prediction by eq 14 with free parameter $A_{CR} = 4.3$.

a single CR event. We expect $A_{CR}b$ to be of order of tube diameter. ref.[7] assumes that for intermediate values of τ_{CR}, the effective friction is given by the sum of two limiting terms. We find that our results can not be fitted with this assumption, but an expression

$$\zeta_{CR}^{tot} = \left(\sqrt{\zeta_0^{cm}} + \sqrt{\frac{2\tau_{CR} k_B T N_{arm} M}{(A_{CR} b)^2}} \right)^2 \tag{14}$$

fits the simulation results very well (solid lines in Figure 9) with $A_{CR} = 4.3$. We also see that the two methods of extracting effective friction give almost identical results within the error bars, which validates our assumption that CR dynamics at very long time scales, of order of $\tau_{CR}Z^2$, is similar to Rouse dynamics. Note however that simulations presented in Appendix A, show that Rouse predictions can not fit the whole stress relaxation curve, because the dynamics at small time scales of order of CR time τ_{CR} deviates from Rouse predictions. If one overlaps small time scales, the functions diverge at the terminal time.

Finally, we need to combine eqs 14 and 10 in the case when only a fraction $1\text{-}\phi_{star}$ of entanglements is blinking with characteristic time τ_{CR}, and the other entanglements are permanent. Reference 7 suggests that in the limit of small τ_{CR} the total chain friction must always remain ζ_0^{cm} independent of $1/\phi_{star}$, whereas, in contrast to eq 14, ζ_{CR}^{tot} becomes dependent on mobile fraction of entanglements through additional chain friction. The following equation satisfies all these requirements:

$$\frac{1}{\zeta_{eff}} + \frac{1}{(\sqrt{\zeta_+} + \sqrt{\zeta_{CR}})^2} = \frac{1}{\zeta_0^{cm}} \Rightarrow \zeta_+ = \frac{\zeta_0^{cm}}{1 - \phi_{star}} \tag{15}$$

where $\zeta_{CR}^{tot} = ((\zeta_+)^{1/2} + (\zeta_{CR})^{1/2})^2$ with ζ_{CR} being infinitesimally small (at $\tau_{CR} \to 0$) and ζ_+ is the additional friction contribution from the chain in the case when only fraction $1\text{-}\phi_{star}$ of entanglements is involved into CR tube motion.

The time-shift factor, $X(\phi_{star})$, between the stress relaxation function of the truly diluted monodisperse star, $G_{star,zone2}(t)$ (eq 6), and that of the star-linear blend, $G_{star}(t)$, can now be obtained by calculating the ratio of corresponding total friction coefficients using components derived in eqs 9, 10, and 15:

$$X = \frac{(\zeta_{tot})}{(\zeta_0^{cm})} = \left(\phi_{star} + \frac{1}{\frac{\zeta_{CR}}{\zeta_0^{cm}} + \frac{1}{1 - \phi_{star}}} \right)^{-1} \tag{16}$$

where ζ_{tot} is the total effective friction coefficient in the fat tube and ζ_0^{cm} is a total friction coefficient of the chain in the skinny tube.

We now plot the predictions of eqs 16 in Figure 10 (solid line) and compare them with the empirical shift factors obtained

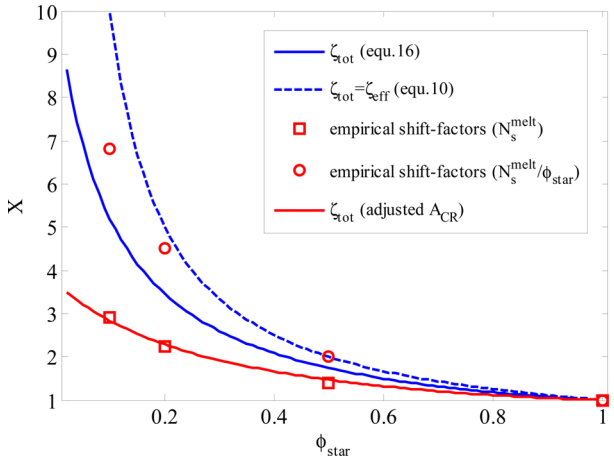

Figure 10. The time shift factors calculated by eq 16 superimposed with the empirically obtained shift factors. Dashed blue line: calculated total FT friction coefficient ζ_{tot} as a bare friction coefficient of the chain (eq 10). Solid blue line: calculated total FT fiction coefficient takes into account total CR friction, ζ_{CR}^{tot} (eq 14). Circles and squares correspond to empirical shift factors obtained for concentration dependent softer slip-links $N_s = N_s^{melt}/\phi_{star}$ and with constant N_s^{melt}, respectively.

earlier (squares in Figure 10). We find that our estimation of the ζ_{CR} predicts higher friction when measured directly by the shift factors. The empirical results however can be fitted very well by eq 16 if A_{CR} is adjusted to $A_{CR} = 11$. There can be at least two reasons for this deviation. First, the friction coefficients ζ_{CR}^{MSD} and ζ_{CR}^{Φ} were measured for three-dimensional motion in free space, with all constraints blinking. In the diluted star simulation, only a fraction of slip-links were blinking, and the friction we are interested in is the friction associated with one-dimensional motion along the fat tube. These might easily be different, as for example shown in ref 3.

The second reason is that the fat tube theory[7] presented here is slightly different from the slip-spring model. In particular, one might imagine that the fat tube would be better modeled with softer slip-springs; i.e., one can change the strength of virtual slip-springs with concentration $N_s = N_s^{melt}/\phi_{star}$. We have performed such simulations, which can also be shifted toward our binary blends simulations. The resulting shift factors are shown in Figure 10 by circles. We see that in this case the fat tube theory underestimates the resulting friction. We find however that such simulations are not consistent with binary blends of linear chains, and therefore we use constant N_s simulations throughout this paper.

In summary, we find that the friction in the fat tube can be adequately predicted by the theory of Read et al.[7] with two modifications: the nonlinear mixing rule (eq 14) and the need to adjust a model-dependent prefactor A_{CR}.

dx.doi.org/10.1021/ma402475a | Macromolecules 2014, 47, 2451−2463

5. CONCLUSIONS

In this study, we have analyzed the relaxation dynamics of star chains in well controlled star/linear blends by comparing quantitative predictions from the slip-spring model to the predictions obtained from various options in tube theory. We separate the relaxation function of the stars in three characteristic time zones. At short times, zone 0 is dominated by Rouse relaxation modes and contour length fluctuations in the skinny tube. At intermediate times, the "skinny" tube (made by all topological constraints) around the star chains explores the "fat" tube (made by long-lived obstacles only). This zone is limited by the time required for exploration of a single fat tube segment by CR Rouse motion of the skinny tube. CR contribution of the star chains themselves in this time zone is found to be small and hence neglected. For most of the blends investigated here, we observe that arm retraction is only slightly affected by CR from linear chains. However this effect is getting more pronounced at low star concentrations (e.g., 2 wt %). Zone 2 corresponds to the stress relaxation of the star chains in the fat tube, and is accompanied by the tube dilation due to CR from other stars. We propose a simple multiplicative mixing law for combining the description of relaxation in the three regions.

It was demonstrated that the effective friction of the star chains in the fat tube is larger than the bare friction of the free chain due to the blinking nature of the star-linear topological obstacles in zone 2. Therefore, the slow relaxation modes of the stars present in the blends are shifted toward longer times compared to the slow relaxation modes of stars diluted in true solvent. Applying this time-shift factor, both star relaxation functions were found to superimpose very well in the terminal regime. The shift factors can at least be semiquantitatively predicted.

In summary, the use of a stochastic model capable of quantitatively predicting chain dynamics at long time scales and validated by comparison with the experimental data is found to be a promising method to investigate fundamental questions and further improve the prediction of the relaxation processes in the framework of tube theory.

APPENDIX A: CONSTRAINT RELEASE RELAXATION FUNCTIONS

In this appendix, we discuss our method for obtaining the constraint release relaxation function $R(t)$ and compare it with other models and analytical expressions. In the slip-spring model, the constraints, modeled by individual slip-springs, are appearing and disappearing at the ends of each chain due to reptation and CLF, but also everywhere along the chain due to CR. To isolate the relaxation due to CR from other mechanisms, we run the slip-spring model without slip, where slip-links are permanently attached to their monomers. This kills reptation, CLF and longitudinal modes inside the tube, leaving only fast Rouse modes and the CR. CR is then modeled by deleting and inserting a fraction ϕ_{fast} of slip-springs (shown in the top inset of Figure 11 with green circles) with the constant rate $1/\tau_{CR}$, i.e., the probability of slip-spring being deleted at each step is dt/τ_{CR}, where dt is the simulation time step. The remainder of slip-springs, shown in Figure 11 with crosses (fraction $\phi_{slow} = 1 - \phi_{fast}$), is permanent and does not blink.

We compute the stress relaxation of such a model (also reported in ref 44 for the case $\phi_{slow} = 0$) and then subtract the fast Rouse modes by fitting the results with a set of Maxwell modes and then subtracting the contribution of all modes with characteristic times smaller than τ_e, and normalize $R(t)$ in such a way that $R(0) = 1$. The results are shown by circles in Figure 11 for $\tau_{CR} = 60$, which is the reptation time of our linear chains, and for the range of concentrations. By definition, all curves start from 1 and go to a long time plateau equal to the fraction of slip-springs which do not blink, ϕ_{slow}. These are the results which were used in the main part to fit the full simulations.

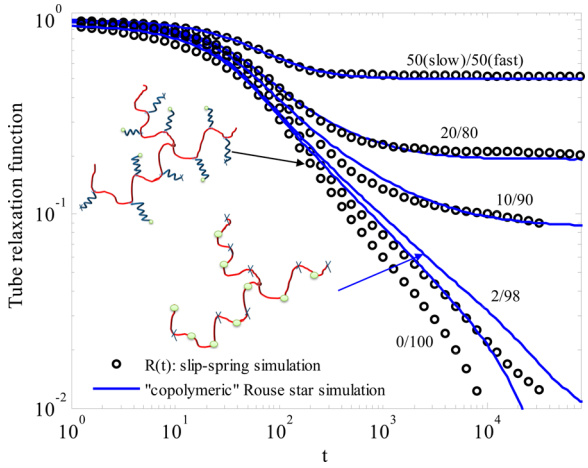

Figure 11. Comparison between slip-spring simulation of the tube relaxation function, $R(t)$, shown by black circles and relaxation function predicted by simulation of a "dual bead" Rouse model (thick blue lines) for a star-shaped chain, with number of entanglements in the first model equivalent to the total number of beads in the second model. Variable fraction of randomly distributed "slow" beads in the "dual bead" Rouse model is equivalent to number of entanglements with infinite lifetime in the slip-spring simulations. All mobile beads in the Rouse model have the same friction, ζ_{fast}, corresponding to lifetime of "fast" entanglements, τ_{CR}, in the slip-spring model.

It is desirable to obtain simpler ways of computing these curves without having to do the simulations for every concentration and CR time. In this Appendix we briefly show a comparison with other simpler methods, none of which is fully adequate in all cases. We leave the derivation of correct analytical solution of this problem to future publications.

First, we simplify the model by removing the virtual springs, and replacing them by beads with different friction coefficients. To this end, we simulate stars made of random copolymer chains with $Z = N/4$ beads per arm. The friction of each bead is selected at random at the beginning of simulation, and it is equal to ζ_{fast} with probability ϕ_{fast} (shown in the lower inset of Figure 11 by green circles) and to infinity (i.e., bead fixed in space, shown in Figure 11 by crosses) with probability $1 - \phi_{fast}$. The simulation results using 1000 chains are shown in Figure 11 by lines. The 0/100 case corresponds to all beads having the same friction, therefore obeying perfect Rouse dynamics. The friction $\zeta_{fast} = 700$ was chosen here to make results overlap at early times. As apparent from simulations with low concentration of slow beads, the long time dynamics of our copolymer model is slower than that of the full slip-springs CR model. Alternatively, one can overlap late times, in which case the copolymer model would predict faster relaxation at early times.

Next, we compare copolymer simulation results with the prediction of Rouse theory for a regular copolymer, where the slow beads are distributed evenly along the chain. In this case the

dx.doi.org/10.1021/ma402475a | Macromolecules 2014, 47, 2451−2463

stress relaxation function is given by

$$R(t) = \phi_{slow} + \phi_{fast}\phi_{slow} \sum_{q=1}^{1/\phi_{slow}} \exp\left(-\frac{24t}{\zeta_{fast} b^2} \sin^2\left(\frac{\pi q}{2\left(\frac{1}{\phi_{slow}} + 1\right)}\right)\right) \quad (17)$$

which is shown in Figure 12 by red lines and compared with random copolymer simulations *(thick blue line)*. We see that the agreement is reasonable apart from the 2% concentration, which contains only about 1 slow bead per star molecule. Finally, ref[15] provides an analytical expression for the random copolymer case:

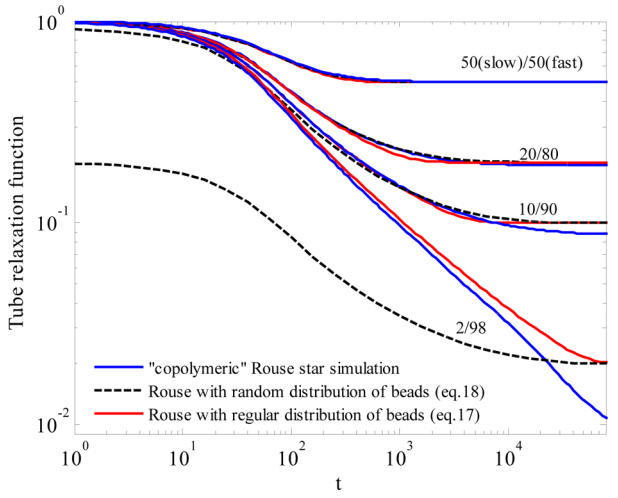

Figure 12. Comparison of stress relaxation function obtained by simulations of unentangled "copolymeric" star chain with those predicted by Rouse theory. Total number of beads per arm is equal to $Z = 19$ for all cases. Ratio of slow beads with infinite friction and fast beads with friction $\zeta_{fast} = 700$ are varying from 50/50 to 2/98. Thick blue line: Simulations results of the star chain with different fractions of randomly distributed fast and slow beads. Dashed black line: Stress relaxation function predicted by eq 18. Fast beads and slow beads are randomly distributed. Red line: Stress relaxation function for the chain with evenly distributed fast and slow beads (see eq 17).

$$R(t) \approx \phi_{slow} + \phi_{slow}^{\ 2} \sum_{n=1}^{2Z} \phi_{fast}^{\ n} \sum_{q=1}^{n} \exp\left(-\frac{24t}{\zeta_{fast} b^2} \sin^2\left(\frac{\pi q}{2(n+1)}\right)\right) \quad (18)$$

which is valid in the limit of very long chains with many slow beads in each chain. We plot this prediction in Figure 12 by dashed black lines. It works pretty well for large ϕ_{slow}, and fails for $\phi_{slow} = 0.1$ and 0.02. In particular, it does not obey the obvious requirement $R(0) = 1$, but satisfies $R(infinity) = \phi_{slow}$. Since the main aim of this paper is to understand the interplay between different physical processes at different time scales, we use $R(t)$ directly simulated from the sip-spring model rather than analytical approximations presented here. This allows us to separate physical assumptions from the mathematical approximations.

APPENDIX B: SLIP-SPRING SIMULATIONS OF MONODISPERSE STARS

In this appendix, we validate simulation results of the slip-spring model by comparison with rheological frequency-sweep experimental data of pure stars published elsewhere. However, we should note that a detailed study of stress relaxation of monodisperse stars including branch point dynamics and possible rules for passing slip-links through the branch point is beyond the scope of this paper. Instead, we propose a method for extending the theory of monodisperse star to the case of star/linear blends by understanding and modeling the effect of constraint release. As complete theory for monodisperse stars is still under development we rely on simulation results validated by rheological experiments. This significantly simplifies our task but also is sufficient to achieve goal of this study.

In Figure 13, we superimpose slip-spring predictions with experimental data of frequency dependent loss and storage moduli for 4-arm star polybutadienes published earlier by Roovers.[45] We constrain the selection of the samples for this validation by the longest accessible computational time of 5 days, which is equivalent to time required for simulation of star chain with ~75 beads/arm.

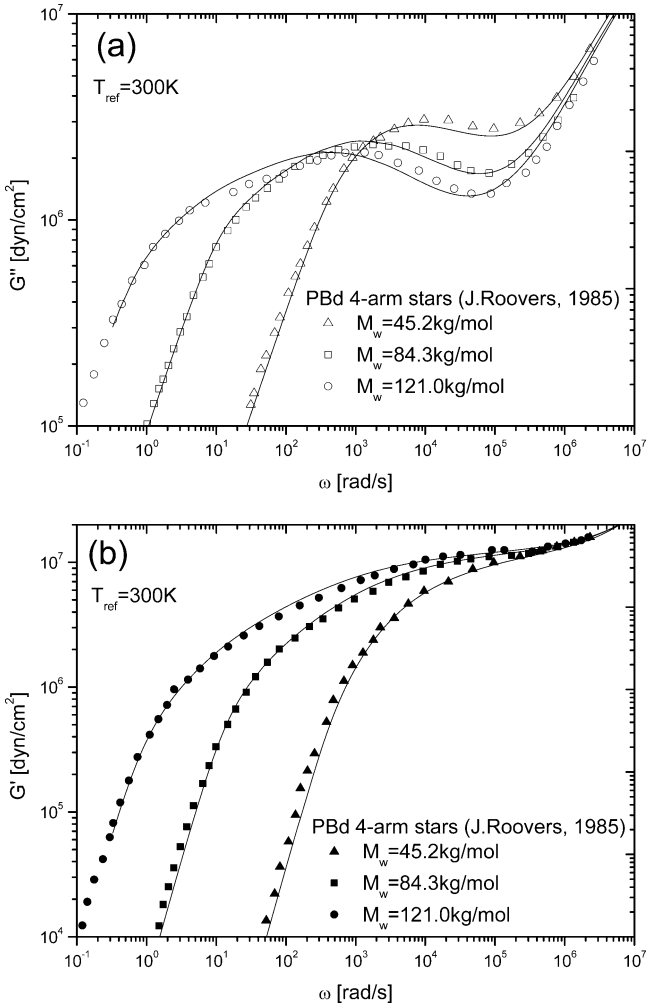

Figure 13. Simulation results of the slip-spring model (solid lines) superimposed with (a) Roovers[45] experimental dynamical storage and (b) loss moduli of monodisperse 4-arm symmetric stars polybutadienes with different molecular weights measured at $T_{ref} = 300$ K (markers). All slip-spring simulations are done with the same parameters: $M_0 = 0.37$ kg/mol, $G_0 = 8$ MPa, and $\tau_0(T_{ref} = 300\ \text{K}) = 3.855 \times 10^{-6}$ s.

In Figure 13, we observe a good match over the whole relaxation time range for all stars. All simulations are done with the same parameters which are in accord with values used in this study. However, a small discrepancy in G_0 and M_0 is observed for

dx.doi.org/10.1021/ma402475a | Macromolecules 2014, 47, 2451−2463

two sets of PBd samples, which can be explained by some differences between the microstructure of samples originating from different laboratories. However deeper analysis including verification of molecular weights would be required to confirm this.

List of Functions

In order to help the reader, we collect functions introduced throughout the text of this paper in the table below.

function	description
$\mu(t)$	simulated fraction of initial tube segments of the star component which are still oriented at time t.
$\mu_{sub}(t)$	simulated fraction of initial tube segments of the star component from which modes slower than $\tau_{e,FT}$ have been subtracted
$\Phi(t)$	simulated end-to-end vector autocorrelation function of the star component in the star/linear blends
$G_{star}(t)$	simulated total stress relaxation function of the star component in the star/linear blends
$R(t,\tau_{d,lin},\phi_{lin})$	simulated stress relaxation function due to constraint release of the star component in the blends
$G_{star,zone1}(t)$	stress relaxation function of the star component in zone 1, predicted as a product of $\mu_{sub}(t)$ and $R(t,\tau_{d,lin},\phi_{lin})$
$G_{star,zone2}(t)$	stress relaxation function of the star component in zone 2, described as the shifted relaxation in the fat tube
$G^{sub}_{star,zone2}(t)$	stress relaxation function of the star component in zone 2 from which fast Rouse relaxation modes have been subtracted
$G_{total}(t)$	theoretical prediction of total relaxation function for the star component in the star/linear blends

AUTHOR INFORMATION

Corresponding Author

*(A.E.L.) E-mail: a.likhtman@reading.ac.uk.

Corresponding author for materials section

#E-mail: Nikolaos.Hadjichristidis@kaust.edu.sa.

Notes

The authors declare no competing financial interest.

ACKNOWLEDGMENTS

We thank Dr. Dietmar Auhl for assistance in experimental part of this work and Prof. Hiroshi Watanabe, Dr. Zuowei Wang, Dr. Yuichi Masubuchi for valuable discussions. We also thank Prof. J. Roovers for providing us with experimental data of the monodisperse star polymers. The research leading to these results has received funding from the [European Community's] Seventh Framework Programme [FP7/2007-2013] under Grant Agreement No. 214627-DYNACOP. Computational resources have been provided by the supercomputing facilities of the Université catholique de Louvain (CISM/UCL).

REFERENCES

(1) de Gennes, P.-G. *J. Chem. Phys.* **1971**, *55*, 572.
(2) Doi, M.; Edwards, S. F. *The Theory of Polymer Dynamics*; Oxford University Press: New York, 1986.
(3) Likhtman, A. E.; Talib, M. S.; Vorselaars, B.; Ramirez, J. *Macromolecules* **2013**, *46*, 1187.
(4) Likhtman, A. E. *Macromolecules* **2005**, *38*, 14.
(5) Likhtman, A. E.; McLeish, T. C. B. *Macromolecules* **2002**, *35*, 6332.
(6) Likhtman, A. E. *Viscoelasticity and molecular Rheology*. In: *A comprehensive Reference*; Elsevier B.V.: Amsterdam, 2012; pp 133−179.
(7) Read, D. J.; Jagannathan, K.; Sukumaran, S. K.; Auhl, D. *J. Rheol.* **2012**, *56*, 823.
(8) van Ruymbeke, E.; Keunings, R.; Bailly, C. *J. Non-Newtonian Fluid Mech.* **2005**, 128.
(9) van Ruymbeke, E.; Bailly, C.; Keunings, R.; Vlassopoulos, D. *Macromolecules* **2006**, *39*, 6248.
(10) Ahmadi, M.; Bailly, C.; Keunings, R.; Nekoomanesh, M.; van Ruymbeke, E. *Macromolecules* **2011**, *44*, 647.
(11) Auhl, D.; Chambon, P.; McLeish, T. C. B.; Read, D. J. *Phys. Rev. Lett.* **2009**, *103*, 136001.
(12) Snijkers, F.; van Ruymbeke, E.; Kim, P.; Lee, H.; Nikopoulou, A.; Chang, T.; Hadjichristidis, N.; Pathak, J.; Vlassopoulos, D. *Macromolecules* **2011**, *44*, 8631.
(13) Larson, R. G. *Macromolecules* **2001**, *34*, 4556.
(14) Das, C.; Inkson, N. J.; Read, D. J.; Kelmanson, M. A.; McLeish, T. C. B. *J. Rheol.* **2006**, *50*, 207.
(15) Rubinstein, M.; Helfand, E.; Pearson, D. S. *Macromolecules* **1987**, *20*, 822.
(16) Struglinski, M. J.; Graessley, W. W. *Macromolecules* **1985**, *18*, 2630.
(17) Struglinski, M. J.; Graessley, W. W.; Fetters, L. J. *Macromolecules* **1988**, *21*, 783.
(18) Graessley, W. W. *Adv. Polym. Sci.* **1982**, *47*, 67.
(19) Wang, S.; Wang, S.-Q.; Halasa, A.; Hsu, W.-L. *Macromolecules* **2003**, *36*, 5355.
(20) Park, S. J.; Larson, R. G. *Macromolecules* **2004**, *37*, 597.
(21) Park, S. J.; Larson, R. G. *J. Rheol.* **2006**, *50*, 21.
(22) Milner, S. T.; McLeish, T. C. B. *Macromolecules* **1997**, *30*, 2159.
(23) Milner, S. T.; McLeish, T. C. B.; Young, R. N.; Hakiki, A.; Johnson, J. M. *Macromolecules* **1998**, *31*, 9345.
(24) Yoshida, H.; Watanabe, H.; Kotaka, T. *Macromolecules* **1991**, *24*, 572.
(25) Lee, J. H.; Fetters, L. J.; Archer, L. A.; Halasa, A. F. *Macromolecules* **2005**, *38*, 3917.
(26) Lee, J. H.; Archer, L. A. *Macromolecules* **2002**, *35*, 6687.
(27) Marucci, G. *J. Polymer science* **1985**, *23*, 159.
(28) Doi, M.; Graessley, W. W.; Helfand, E.; Pearson, D. S. *Macromolecules* **1987**, *20*, 1900.
(29) Lin, Y.-H. *Macromolecules* **1989**, *22*, 3075.
(30) Ball, R. C.; McLeish, T. C. B. *Macromolecules* **1989**, *22*, 1911.
(31) de Gennes, P.-G. *Macromolecules* **1976**, *9*, 587.
(32) Klein, J. *Macromolecules* **1978**, *11*, 852.
(33) Daoud, M.; de Gennes, P.-G. *J. Polym. Sci., Polym. Phys. Ed.* **1979**, *17*, 1971.
(34) Watanabe, H.; Matsumiya, Y.; Osaki, K. *J. Polym. Sci., Part B: Polym. Phys.* **2000**, *38*, 124.
(35) Matsumiya, Y.; Watanabe, H. *Macromolecules* **2001**, *34*, 5702.
(36) Watanabe, H.; Matsumiya, Y.; Inoue, T. *Macromolecules* **2002**, *35*, 2339.
(37) Watanabe, H. *Kor.-Austr. Rheol. J.* **2001**, *13*, 205.
(38) Watanabe, H.; Ishida, S.; Matsumiya, Y.; Inoue, T. *Macromolecules* **2004**, *37*, 1937; **2004**, *37*, 6619.
(39) Viovy, J. L.; Rubinstein, M.; Colby, R. H. *Macromolecules* **1991**, *24*, 3587.
(40) Ferry, J. D. *Viscoelastic Properties of Polymers*, 3rd ed.; Wiley: New York, 1980.
(41) Fox, T. G.; Flory, P. J. *J. Appl. Phys.* **1950**, *21*, 581.
(42) Kelley, F. N.; Bueche, F. *J. Polym. Sci.* **1961**, *50*, 549.
(43) Hadjichristidis, N.; Iatrou, H.; Pispas, S.; Pitsikalis, M. *J. Polym. Sci.—Polym. Chem.* **2000**, *38*, 3211.
(44) Read, D. J.; Jagannathan, K.; Likhtman, A. E. *Macromolecules* **2008**, *41*, 6843.
(45) Roovers, J. *Polymer* **1985**, *26*, 1091.
(46) Ramirez, J.; Sukumaran, S. K.; Likhtman, A. E. *J. Chem. Phys.* **2007**, *126* (24), 24490.